Structural, Optical and Electronic Properties of Hydrogenated SiC Films Prepared by Magnetron Sputtering Method

Nobuo SAITO [a)]

Abstract

Physical properties of semiconductors are much more changed by disorder than metals or insulators, and are the most interesting field for fundamental research. The author has studied on several kinds of disordered semiconductor films. One of the author's contributable materials to this field is hydrogenated amorphous SiC (a-SiC:H) prepared by magnetron sputtering (MSP) of silicon in methane-argon gas mixtures. In this article, the author describes the methods of film deposition, physical properties, their merits, limitations and achievements.

The first chapter deals with the fundamental properties of a-SiC:H deposited using methane gas which is considered essential for any deeper understanding of the nature of the films. The second chapter is the effects of sputtering conditions on the film properties. The third chapter deals with doping effects deposited by co-sputtering or reactive-one. The fourth chapter is the formation of partly micro crystallized films which are considered difficult to shift from the amorphous state. The last chapter deals with the formation of the superlatice structure composed of a-SiC:H and a-GeC:H multilayers.

Keywords: SiC, Film, Sputtering, Amorphous, Micro crystal, Superlatice

CHAPTER 1

1.1 Introduction

In this chapter, the fundamental properties of hydrogenated amorphous silicon carbon (a-SiC:H) films prepared by MSP in CH_4-Ar gas mixtures is introduced[1)]. During recent years, the work on a-SiC:H alloy films prepared by the glow-discharge (GD) decomposition of silane and a hydrocarbon, like methane or ethylene, has made a useful contribution to the development of amorphous materials[2,3)], and also that of opto-electronic devices like solar cells. On the other hand, there are few reports of devices using a-SiC:H prepared by the sputtering (SP) method, because the opto-electronic properties of SP a-Si:H films are inferior to those of GD a-Si:H[4,5)]. However, it is important to investigate SP a-SiC:H from the standpoint of both a fundamental understanding and of opto electronic device applications such as photo sensors, electro photography and image tubes using films having wider optical gaps than a-Si:H.

In the case of the SP method, there are several varieties of the source of material: (i) SiC target and a gas mixture of hydrogen and argon[6,7)]; (ii) composite target of silicon and graphite and the same gas mixture as (i)[8–11)]; and (iii) silicon target and hydrocarbon-argon gas mixture[9,10)]. Though the optical and structural properties of SP a-SiC:H alloy films are reported in these papers, there are few reports of the electrical properties[7)]. In this chapter, the author reports on the opto-electronic properties, as well as the optical and the structural properties, of SP a-$Si_{1-x}C_x$:H prepared by method (iii) using a magnetron sputtering (MSP) system. Using this apparatus, SP a-Si:H films could be produced with much better opto-electronic properties than can be obtained using conventional sputtering techniques[12)] .

1.2 Experimental details

(1) Sample preparation

The a-$Si_{1-x}C_x$:H films were prepared using an rf diode MSP apparatus. The magnetic flux density at the vicinity of the Si target (99.999%; 100 mm in diameter and 5 mm in thickness) was about 300 G. Two types of substrate were used: one was a high-resistivity silicon wafer with a resistivity of more than 1000 Ω cm; the other was a fused-quartz plate. The former substrate was used for the infrared measurements, and for other measurements the latter was used. The distance between the target and the substrates was 45 mm. The sputtering chamber was evacuated below 10^{-6} Torr before the introduction of methane and argon through variable-leak valves. The target was cleaned by pre sputtering for more than 30 min before the deposition of the film, and the sputtering pressure used was 7 mTorr. The substrate temperature was held at 300 °C, and the rf power was 200 W during the deposition. The carbon content in the film was varied by varying the partial pressure of methane with respect to the total gas pressure.

Aluminum electrodes were deposited on to the amorphous films in a coplanar gap cell configuration using a photocell mask with a gap of 0.3 mm and a width of 90 mm.

(2) Measurements and results

The film composition was determined using an electron-probe microanalyser (Shimazu: EMX SM7). The thickness of the deposited film was measured with a stylus instrument (Sloan: Dektak), and the

a) Professor, Dept. of Applied Physics

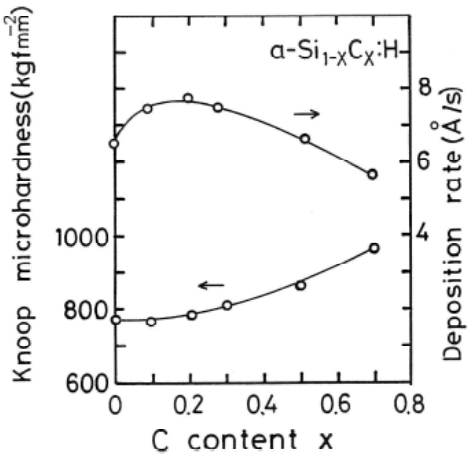

Fig. 1-1. Deposition rate and Knoop microhardness as a function of carbon content x.

deposition rate is shown in Fig.1-1 as a function of x.

The values are larger than in the case of the conventional SP method using a composite target[8]. This is due to both the effect of the magnetron SP method and the use of methane gas as a source of carbon instead of graphite, where the sputtering yield is less than one half of silicon. The dark conductivity and the photoconductivity were measured in a cryostat evacuated below 10^{-5} Torr. The photoconductivity was obtained as the difference between the dark conductivity and the conductivity when illuminated by a He-Ne laser with a photon flux of 5.7×10^{15} cm^{-2} s^{-1}.

The transmittance and the reflectance spectra in the wavelength range of 200–900 nm were measured by a double-beam spectrophotometer (Jasco: Uvidec 505). The absorption coefficient was obtained from these spectra by the same method as reported in a previous paper[12]. The transmittance spectrum in the wave number range of 400–4000 cm^{-1} was measured with a double-beam spectro photometer (Jasco: A202). The absorption coefficient was obtained from the spectrum and the hydrogen concentration N was calculated from the relation $N = AI_a$, where I_a is the integrated absorption coefficient and A is a constant. The values A used in this study are 1.4×10^{20} cm^{-2} for the calculation of hydrogen bonded to silicon[13], and 1.0×10^{21} cm^{-2} for that of hydrogen bonded to carbon[14].

The Knoop micro hardness was measured by a micro hardness tester (Akashi MVK-E) fitted with a Knoop diamond indenter. The load used was 10 g and the holding time under load was 30 s. Although the gradual increase in the micro hardness with increasing x, shown in Fig.1-1, is associated with the increase in the proportion of Si-C bonds, the value at $x = 0.5$ is lower than that of crystalline silicon carbide (2000–4000 kg mm^{-2}). According to the interpretation by Bayne et. al.[15], this may be

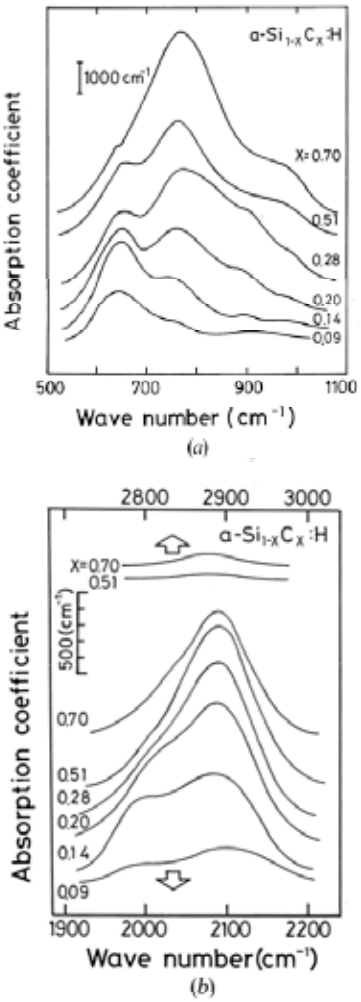

Fig. 1-2. Variation in IR absorption spectrum with x in the range of (a) 500–1200 cm^{-1} and (b) 1900–2200 and 2800–3000 cm^{-1}.

due to the C-Hn bonds described later.

1.3 Results and discussion

(1) IR spectra

Figure 1-2 (a) shows the variation in the IR absorption spectrum with x in the range 500–1200 cm^{-1}. The spectrum mainly consists of two absorption bands: one is the 630 cm^{-1} band; the other the 780 cm^{-1} band. The former is the well-known Si-Hn and (Si-H$_2$)n wagging mode, and the latter the Si-C stretching mode. In addition to these bands, several small peaks are observed: Si-H$_2$ scissors and (Si-H$_2$)n scissors (890 cm^{-1}), and the C-H wagging and/or rocking mode (980 cm^{-1})[2,16].

With increasing x, the carbon-originated absorption bands become recognizable; in particular the intensity of the band due to the Si-C stretching mode increases in the range of x above 0.3.

The variation in the absorption spectrum with x in the range 1900–2200 cm^{-1} is shown in Fig.1-2(b) where the Si-H stretching mode (2000 cm^{-1}) and the Si-H$_2$ stretching mode (2100 cm^{-1}) have been assigned in a-Si:H. With increasing x, the absorption

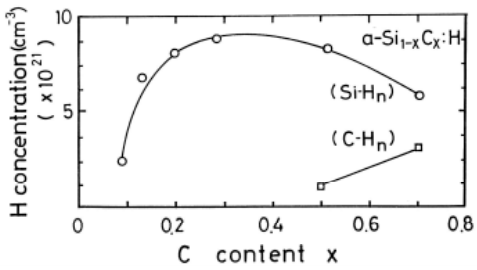

Fig. 1-3. Concentration of hydrogen bonded to silicon or carbon determined from Fig.1-2.

band around 2100 cm^{-1} becomes dominant. In the case of x = 0.7, it is observed that the absorption peak due to the Si-H bond shifts towards a higher wave number owing to the increase in the number of Si-C bonds.

Figure 1-3 shows the concentration of hydrogen bonded to silicon or carbon. The results in Fig. 1-3 imply that methane is sufficiently decomposed and that the use of methane instead of hydrogen is effective as a source of hydrogen in the range of x above 0.2. The gradual decrease in the concentration of hydrogen bonded to silicon with increasing x above 0.5 is related to the increase in the number of C-Hn bonds as well as Si-C bonds.

The absorption band around 2900 cm^{-1} corresponding to the C-Hn stretching modes shown in Fig.1-2 was too weak in films below x = 0.5 to calculate the amount of hydrogen bonded to carbon, though it has been observed clearly in GD films[2,16]. The small amount of hydrogen bonded to carbon in our films as seen in Fig.1-3 is ascribed to the deposition conditions in our SP method; the pressure during the deposition is at least one order of magnitude lower and the rf power about one order magnitude larger than the general conditions in the GD method. These conditions in the MSP method will make methane more unstable towards decomposition than those used in the GD method. In other words, it is suggested that in the films prepared under these conditions the ratio of C-H bonds to $C\text{-}H_2$ and $C\text{-}H_3$ bonds is larger than that found in conventional GD-produced films.

(2) Optical absorption spectra

Figure 1-4 shows the optical absorption spectra plotted as $(\alpha h\nu)^{1/2}$ versus photon energy $h\nu$, according to the relation analyzed by Mott and Davis[17]: $\alpha h\nu = B\,(h\nu - Eo)^2$, where α is the absorption coefficient, B a constant and Eo the optical band gap. The optical absorption spectrum shifts towards higher photon energy with increasing x without changing the slope B of the spectrum, except for the case of x = 0.7.

The constant B is proportional to $N(E)^2/n\Delta E$ where $N(E)$ is the density of states at the band edge, n the refractive index and ΔE the condition band tail

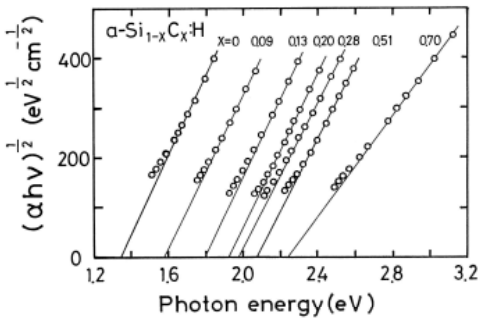

Fig. 1-4. Variation in optical absorption plotted as $(\alpha h\nu)^{1/2}$ versus $h\nu$ as a function of x.

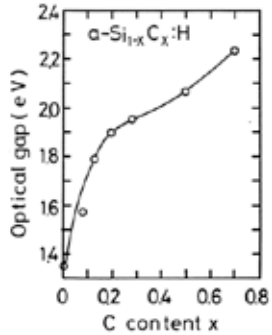

Fig. 1-5. Compositional dependence of the optical band gap Eo.

width[17]. As it has been reported[18,19] that n decreases with increasing x; ΔE in our films will increase if $N(E)$ is unchanged. The optical band gap Eo is obtained by fitting the absorption data shown in Fig. 1-4 to the above expression. Figure 1-5 shows the dependence of the optical band gap on x. The rapid increase of Eo in the range of x below 0.2 is mainly due to the rapid hydrogenation of silicon as seen in Fig. 1-2. The increase of Eo in the range of x above 0.3 is due to the increase in the number of Si-C bonds. The decrease of the slope B in the case of x = 0.7 may relate to the formation of graphite-like structures and/or to the change of the bonding configuration of carbon caused by an increase in C-Hn bonds.

The phenomenon reported by Shimada et al.[13] that Eo decreases with increasing x above 0.4 owing to the decrease of B in the SP films was not observed in this study. It has been also reported that the peak in Eo exists near x = 0.7 in GD films[18–22]. Unfortunately, the presence of such a peak in Eo was not found in this study, as the largest value of x obtained by our method is 0.7. Setting aside the question of this peak, the use of methane as the source of carbon instead of a graphite target is effective for the control of the optical band gap in SP a-SiC:H films.

(3) Electrical and opto-electronic properties

Figure 1-6 shows the dark conductivity σ_d as well as the normalized photoconductivity $\eta\mu\tau$ as a

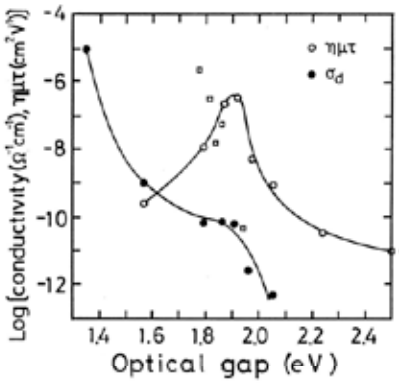

Fig. 1-6. Normalized photoconductivity $\eta\mu\tau$ for a photon energy of 1.96 eV (○) in the present work and (□) after Bullot et al.[3] and Catherine and Turban[18], together with (●) the dark conductivity at room temperature, as a function of the optical band gap.

function of E_o at 294 K, where η is the quantum efficiency, μ the electron mobility and τ the electron lifetime[21]. σ_d decreases monotonically with increasing E_o owing to the hydrogenation of silicon for small E_o and to the increase in the number of Si-C bonds for large E_o, according to the results of the temperature dependence of the dark conductivity[22]. On the other hand, $\eta\mu\tau$ shows a maximum at about E_o = 1.8 eV.

With increasing E_o, up to 1.8 eV, $\eta\mu\tau$ increases rapidly owing to the hydrogenation of silicon. The decrease in $\eta\mu\tau$ with increasing E_o above 1.9 eV cannot be explained only by a mismatch between the optical band gap and the energy of illumination, because AM1 photoconductivity also decreases with increasing x[22]. The decrease in $\eta\mu\tau$ is consistent with the results of GD films[3,21]. This phenomenon has been interpreted as being due to the increase of disorder or of dangling bonds in a-SiC:H films compared to a-Si:H[3,23]. According to this interpretation, the density of localized states will be reduced if the bonding structure among silicon, carbon and hydrogen is more simple or approaches that of an ideal hydrogenated silicon-carbon alloy with a tetrahedrally bonded structure. The values of $\eta\mu\tau$ in the range of E_o above 1.9 eV are larger than the results of the GD films prepared using the gas mixture of methane and silane[3] as seen in Fig. 1-6. This is ascribed to the fairly simple bonding structure between carbon and hydrogen as described in section 1-3(1). In other words, it is suggested that the density of localized states can be reduced in the films having a monomer-like C-H bonding structure compared to those with polymer-like ones.

Figure 1-8 shows the activation energies of the photoconductivity E_p and the dark conductivity E_d, obtained from the activated conduction region in the temperature dependence of the dark conductivity[22] and of the photoconductivity shown in Fig.1-7. If

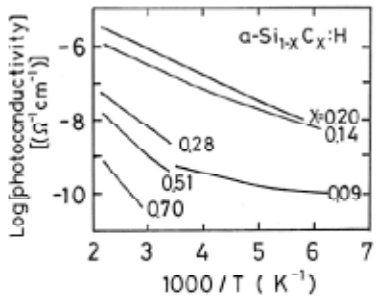

Fig. 1-7 Temperature dependence of the photoconductivity.

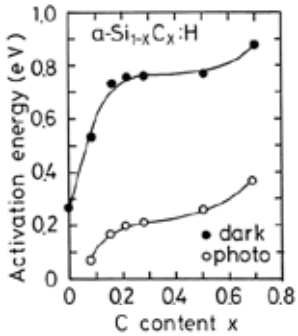

Fig. 1-8 Activation energy of the dark conductivity together with that of the photoconductivity as a function of x.

we assume that the carriers are mainly electrons in our alloy films as in a-Si:H, and that the photo-induced electrons are due to band-to-band excitation, $E_d = E_C - E_F$ and $E_p = E_C - E_A = \Delta E$ where E_F, E_C and E_A are the Fermi level, the mobility edge of the extended conduction states and the edge of the conduction band tail, respectively[24]. The increase of E_d with increasing x is almost in agreement with the results for the optical band gap. E_d is about 0.2 eV smaller than one half of E_o in the whole x range except for x = 0, similar to the general SP and GD a-Si:H films which show weak n-type conduction. The gradual increase in E_p with increasing x, which means a slight widening of the conduction-band tail width, is also in agreement with the tendency deduced from the value B, as discussed in section 1-3 (2). In the case of x = 0.7, the rapid increase in E_p is related to the rapid decrease in both the value B and the refractive index.

It is suggested from the results of this study that a further increase of the photoconductivity might be possible for films having a high concentration of carbon, if the bonding structures between the constituent elements can be optimized by the reaction process between these elements being well controlled by the deposition conditions in the MSP method.

CHAPTER 2 Effects of deposition conditions

2.1 Effects of rf power [25)]

In chapter 1, the author reported that highly photoconductive SP a-SiC:H could be obtained by the use of methane as the sources of hydrogen and carbon in SP a-SiC:H alloy films, and suggested that the larger rf power density in this method than in the GD method is responsible for the excellent optoelectronic properties. This chapter deals with the effects of deposition conditions; especially, the rf power dependence of the structural, optical, electrical, and optoelectronic properties of the material prepared by this method.

2.2 Experiment

For each deposition the vacuum chamber was evacuated to < 7×10^{-7} Torr prior to the introduction of a gas mixture of methane and argon through a variable leak valve. In the present chapter, rf power was varied from 50 to 200 W. Substrate temperature and sputtering pressure were 300 °C and 7 mTorr for each deposition, respectively.

The amorphous nature of the films was certified by RHEED and X-ray diffraction analysis.

2.3 Results and discussion

(1) composition and deposition rate

The carbon contents x in a-$Si_{1-x}C_x$:H are shown in Fig. 2-1 together with the deposition rate, as a function of rf power. The value of x increases rapidly with decreasing rf power. This tendency is consistent with a report for a-SiC:H films prepared by the conventional SP method[26)], where the film composition was determined by Rutherford back scattering. The increase in x with decreasing rf power may be ascribed mainly to the decrease in the sputtering rate of silicon, because it is considered that the silicon target is sputtered mainly by argon ions rather than such species having small sputtering yield as hydrogen ion and hydrocarbon ions produced from methane. The deposition rate r shown in Fig. 2-1 follows a power law dependence on rf power p: $r = ap^n$. The exponent n is about 1.5 and is in good agreement with a reported value for SP a-Si:H[27)] as shown in the figure.

(2) IR spectra and hydrogen concentration

Figure 2-2 shows the variation in IR absorption spectrum with rf power. With decreasing rf power, the carbon-originated absorptions such as the Si-C stretching band at about 780 cm^{-1}, the C-H wagging band at about 1000 cm^{-1} and the C-H stretching bands at about 2900 cm^{-1}, which are not illustrated in this figure, become recognizable. Especially the intensity of Si-C stretching band increases rapidly, and its peak moves toward higher wave number, owing to the increase in the sum of the electro

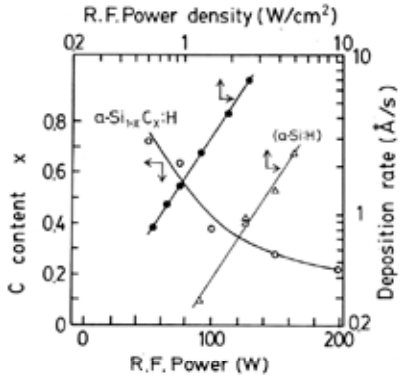

Fig. 2-1. (○) Carbon content x, (●) deposition rate of SP a-$Si_{1-x}C_x$:H films and (△) deposition rate of SP a-Si:H films[27)], as a function of rf power.

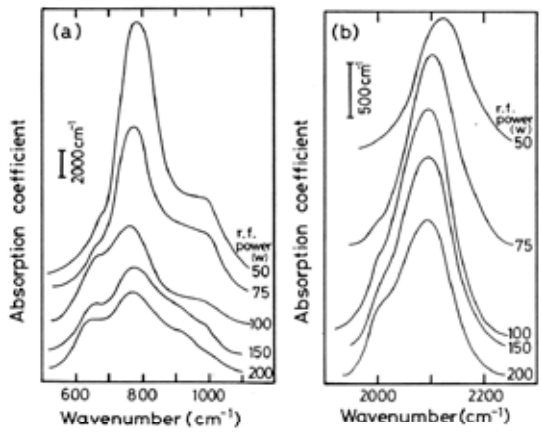

Fig. 2-2. Variation in IR absorption spectrum with rf power in the range of (a) 500–1200 cm^{-1} and (b) 1900–2300 cm^{-1}.

negativity around the silicon atoms[28)]. This effect also results in the upward shift of absorption peak such as Si-Hn wagging bands at about 630 cm^{-1} and Si-H_2 stretching band at about 2100 cm^{-1}. The decrease in the intensity of Si-H stretching band at 2000 cm^{-1} with decreasing rf power may be also ascribed to this effect.

Figure 2-3(a) shows the concentration of hydrogen bonded to silicon (N_{Si-H}) and that bonded to carbon (N_{C-H}), estimated from IR spectra. With decreasing rf power, N_{C-H} increases rapidly owing to the decrease in the degree of decomposition of methane, whereas N_{Si-H} shows a maximum which may be ascribed to an optimum condition in the reaction process among such species in the plasma as atoms, radicals, and ions composed of silicon, hydrogen, and hydrocarbon.

The hydrogen bonding ratio of silicon N_{Si-H}/N_{Si} and that of carbon N_{C-H}/N_C are shown in Fig. 2-3(b) as a function of rf power, where N_{Si} and N_C are the concentrations of Si and of C, respectively. Both ratios tend to increase with decreasing rf power, though N_{Si-H}/N_{Si} shows a weak maximum, reflecting

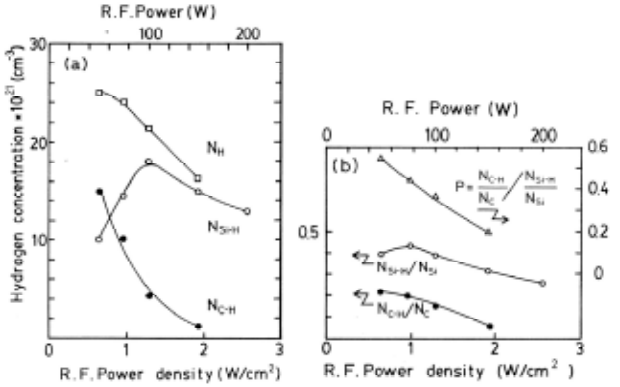

Fig. 2-3. (a) Concentration of hydrogen bonded to (○) silicon. and to (●) carbon, and (□) total concentration of hydrogen, deduced from the stretching bands in ir absorption spectra. (b) Hydrogen bonding ratio of (○) silicon and of (●) carbon. and (△) the factor of preferential attachment of hydrogen to carbon.

a peak in $N_{Si\text{-}H}$. As seen in the figure, $N_{C\text{-}H}/N_C$ is smaller than $N_{Si\text{-}H}/N_{Si}$ in the whole range of rf power investigated. This result is quite different from a report for GD films prepared using a gas mixture of silane, ethylene, and hydrogen; the former is larger than the latter owing to the presence of complicated polymer-like structures in the film originating from hydrocarbon species in the plasma[29]. This difference is ascribed to the difference of deposition process between GD method and the present SP method; in the GD method, the decomposition energies of silane are generally smaller than those of hydrocarbon[30] and rf power density in GD method is generally about one order of magnitude smaller than that in the present SP method. These conditions in the GD method result in the smaller degree of decomposition of hydrocarbon than that of silane in the plasma, and thus consequently in the large amount of hydrogen bonded to carbon in the films.

The factor of preferential attachment of hydrogen to carbon defined by $P = (N_{C\text{-}H}/N_C)/(N_{Si\text{-}H}/N_{Si})$ increases gradually with decreasing rf power, which may be partly responsible for the decrease in the photoconductivity described later. The values of P are remarkably smaller than a report for GD films (2.1–5.1) prepared using a gas mixture of silane and methane[23]. This implies that methane is sufficiently decomposed in the present SP method compared with such a GD method. The values of P are also smaller than report for SP films (1.1–3.6) prepared by the conventional SP system using a composite target of silicon and carbon in a gas mixture of hydrogen and argon[23]. This suggests that the bonding structures between carbon and hydrogen in the present films are relatively simple compared with the conventional SP films, considering the fact that the values of $N_{Si\text{-}H}/N_{Si}$ in the present films are almost in agreement with those reported in Ref.23.

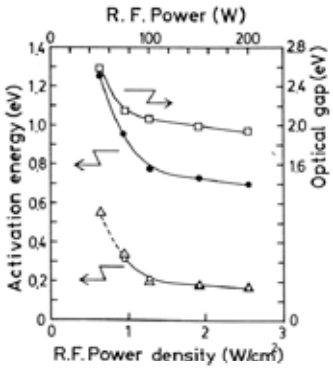

Fig. 2-4. (□) Optical band gap. and activation energies of (●) dark conductivity and (○) photoconductivity, obtained from temperature dependence of conductivity in Fig. 2-6. (△) Width of the conduction-band tail deduced from the optical measurements (see text).

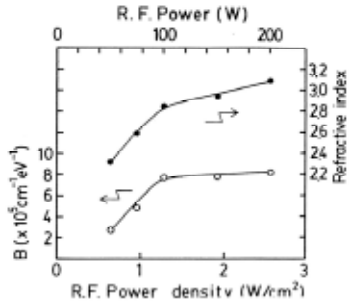

Fig. 2-5. (●) Refractive index and (○) the value of B in the optical absorption spectrum.

It is suggested from these results that an idealized bonding structure between the constituent elements might be formed by the present SP method, which results in the films having high photoconductivity and photosensitivity due to relatively small density of disorder or of dangling bonds, if the chemical reaction mechanism between the species generated in such reaction processes as physical sputtering of silicon, chemical decomposition of methane are well controlled by adjusting the several deposition conditions.

(3) Optical, electrical and opto-electronic properties

Rf power dependence of the optical band gap E_o is shown in Fig. 2-4. With decreasing rf power, E_o increases gradually, owing mainly to the increase in the concentration of Si-C bonds, accompanied with the gradual decrease in B as shown in Fig. 2-5. In this figure the rf power dependence of the refractive index near 300 nm is also shown. The decrease in B implies the increase in the disorder of amorphous structure and the consequent increase in the band tail width as described later.

Figure 2-6 shows the temperature dependence of dark conductivity σ_d as well as photoconductivity σ_p. The activation energies of the photoconduc-

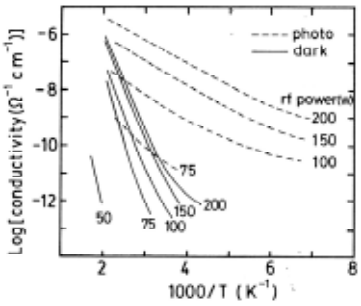

Fig. 2-6. Temperature dependence of dark conductivity and photoconductivity.

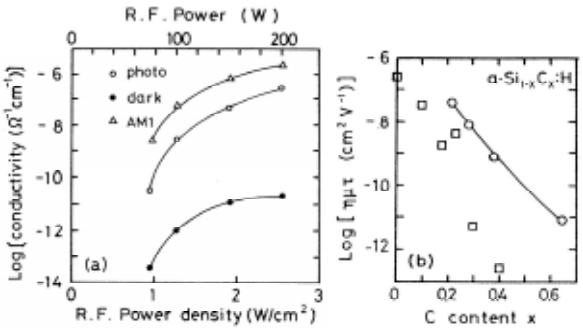

Fig. 2-7. (a) rf power dependence of (●) dark conductivity, and photoconductivity under (○) photon energy of 1.96 eV and photon flux of 5.7×10^{15} cm^{-2} s^{-1} and under (△) AM1 at room temperature (294 K). (b) Normalized photoconductivity at photon energy of 1.96 eV at room temperature, as a function of x. (○) Present results (294 K), (□) GD films prepared using silane-methane gas mixtures[3].

tivity (E_p) and of the dark conductivity (E_d) are shown in Fig. 2-4 as a function of rf power, obtained from the activated conduction region in Fig. 2-6, except for E_p in the case of 50 W. E_d increases with decreasing rf power, in the similar manner to Eo, owing mainly to the increase in the concentration of Si-C bonds.

Calculated values of ΔE are also shown in Fig. 2-4, deduced from the relation described in section 1-3(2): $B = KN(E)^2/n\Delta E$, assuming that for each film $KN(E)^2$ equals to a value of 4.2×10^5 cm^{-1} obtained in the case of 200 W. The calculated values ΔE are in good agreement with E_p. Thus, E_p in the case of 50 W is estimated to be equal to ΔE, on the assumption that the dispersion of the refractive index between 300 nm and 630 nm is negligibly small, in addition to the above assumptions.

The increase in E_p and in the ratio of E_p to Eo with decreasing rf power implies the increase in the disorder of amorphous structure, originating from the increase in the several kinds of quantities relating to the concentration of hydrogen described above, and/or from the change of coordination number of some parts of carbon atoms from four to three[8,19].

With decreasing rf power, σ_d as well as σ_p decreases rapidly, as seen clearly in Fig. 2-7(a). Although the decrease in σ_d is ascribed mainly to the increase in the number of Si-C bonds, which results in the fact that the measurements were difficult near room temperature in the case of 50 W as seen in Fig. 2-6, the decrease in σ_p cannot be explained only by a mismatch between the optical band gap Eo and the energy of illumination (1.96 eV), because the photoconductivity under the illumination of AM1 also decreases with increasing Eo in the same manner as the chapter 1.

According to the interpretation of the decrease in σ_p with increasing x or Eo for GD films[3,22], the increase in the density of dangling bonds or disorder, which is also due to the compositional and/or structural change of films described above, may be responsible for the decrease in σ_p with decreasing rf power in the present study. The photoconductivities are larger than reported values of GD films[3] in the range of x above 0.2 or of Eo above 1.9 eV, as shown in Fig. 2-7(b) where the data are plotted as normalized photoconductivity $\eta\mu\tau$. From the interpretation described above, this suggests that the density of dangling bonds or of defects are relatively small in the present films compared to GD films.

2.4 Effects of other deposition conditions

The author has reported also the effects of several deposition conditions such as, (1) sputtering pressure[31], (2) addition of hydrogen gas[32], (3) variation of hydrocarbon gas[33] and (4) fluorinated films using CF_4 gas[34]. The results and discussions in detail can be found in these references.

CHAPTER 3 Doping effects

3.1 Impurity doping (Aluminum) [35]

The effects of incorporating impurity atoms of groups III and V into a-Si:H from the solid phase by SP have been studied by several groups[36–41]. Although control of the optical and electronic properties of a-Si:H films has been tried from the standpoint of substitutional doping in these studies, we are unaware of any data on photoconductivity and photosensitivity. This may be due to their small values, as mentioned in some of the papers[37,41]. Moreover, we also cannot find any reports on the effect of incorporation of these impurities into silicon-based hydrogenated amorphous semiconducting alloys such as a-SiC:H and a-SiGe:H using the co-sputtering method. In this chapter, the author reports the effect of imurity doping (aluminum) on the optical and electrical properties of SP a-SiC:H films.

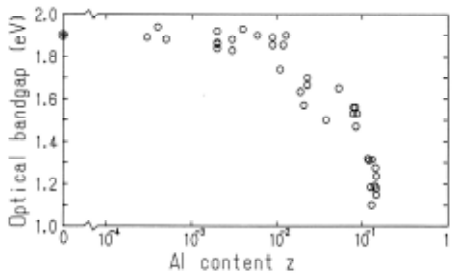

Fig. 3-1 Optical band gap E_o as a function of aluminum content z.

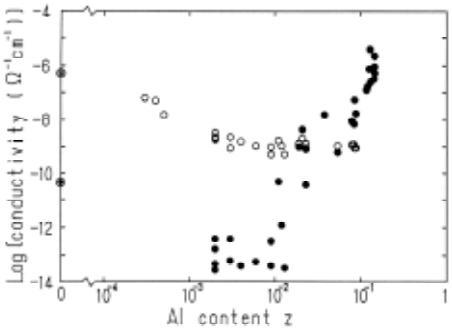

Fig. 3-2 D.c. conductivity σ_d (●) and photoconductivity σ_p (○) (for a photon flux of 5.7×10^{15} cm^{-2} s^{-1} and a photon energy of 1.96 eV) at room temperature (294 K). σ_d for $10^{-4} < z < 10^{-3}$ is smaller than 10^{-14} S cm^{-1}, which is the detection limit of the measuring system.

3.2 Experiment

Films were prepared by MSP of a composite target of silicon-aluminum in an atmosphere consisting of a gas mixture of methane and argon. The apparatus and procedure are the same as those adopted for undoped a-SiC:H films which have highly photoconductive and photosensitive properties[1,25,42]. The aluminum content of the film was varied by putting a suitable number of aluminum chips on a silicon target. The film composition was determined using an X-ray probe microanalyser (EPMA).

3.3 Results and discussion

Figure 3-1 shows the dependence of the optical band gap E_o on the aluminum content z. It can be seen that E_o is almost unchanged on increasing z up to 10^{-2}. This implies that, in this range of z, the aluminum is incorporated in the amorphous network as a substitutional dopant. E_o decreases rapidly with increasing z above 10^{-2}, suggesting the formation of an alloy when the concentration of aluminum is too high to be incorporated into the amorphous network as a dopant.

Figure 3-2 shows the d.c. conductivity σ_d measured at room temperature (294 K). The z dependence of the photoconductivity, σ_p, measured under a photon flux of 5.7×10^{15} cm^{-2} s^{-1} at a photon energy of 1.96 eV is also shown in the figure. When aluminum was introduced into the films, σ_d decreased rapidly down to a level below the detection limit of 10^{-14} S cm^{-1} in the range of z below 10^{-3}. This decrease in σ_d compared with that of undoped films is accompanied by an increase in the activation energy. This implies a movement of the Fermi level toward the valence band, because undoped a-SiC:H shows weak n-type conduction. σ_d increases rapidly with increasing z above 10^{-2}, which is clearly correlated with the rapid decrease of E_o. The increase in σ_d is also accompanied by a decrease in the activation energy. According to a tentative measurement of thermoelectric power, a sample with $z = 3\times10^{-2}$ shows p-type conduction.

The samples were photoconductive in the range of z up to 10^{-1}. In particular, a high value of σ_p of the order of 10^{-8} S cm^{-1} was observed in the range of z below 10^{-3}. In the range of z above 10^{-3} however, σ_p decreases slowly with increasing z. Aluminum does not seem to be incorporated as a separate phase, because if this were so a rather drastic decrease in the lifetime of photo-excited electrons might be expected, as reported for a-Si:H[41].

The photosensitivity, defined as σ_p/σ_d, is about 10^4 for undoped a-SiC:H, and remains at almost this level even with the incorporation of aluminum near to 10^{-2}. The maximum photosensitivity obtained in the range $10^{-4} < z < 10^{-3}$ is estimated to be about six orders of magnitude, if we take a value for σ_d of 10^{-14} S cm^{-1}. These results suggest that this material could be used as a sensitive photo-sensor which requires both a high resistivity and a wide optical band gap.

3.4 Effects of other dopants

The author has reported the detailed data for aluminum doping[43], also the effects of several dopants such as, (1) galium[44], (2) indium[45], (3) thallium[46], (4) bolon[47], (5) antimony[48] and (6) nitrogen[49]. The results and discussions in detail can be found in these references.

CHAPTER 4 Micro-crystallization [50]

4.1 Introduction

Research on the crystallization of films with a tetrahedrally coordinated bonding structure has been active since the effectiveness of micro-crystalline (μc) films as the intrinsic layer of a pin-type solar cell was reported[51]. Much of this research has focused on improving the conversion efficiency of a-Si:H solar cells. Control of the optical bandgap E_o also plays an important role in these materials. There has been aggressive research involving tetrahedrally bonded amorphous semiconductors compos-

ed of Si-C or Ge-C. The formation of such binary materials is possible by changing the *E*o of a-Si:H (for which *E*o is typically 1.7 eV). We have reported basic data on the optical and electrical properties of a-SiC:H or a-GeC:H films with modified band gaps, which were prepared by reactive MSP[52–54], and have compared these data with data from a narrow bandgap material: a-GeC:H[55].

In recent years, research involving μc tetrahedrally bonded binary semiconductor materials such as μc-SiC, SiGe, and GeC has been reported[56–60]. In these studies, experimental deposition methods have mainly focused on plasma enhanced chemical vapor deposition (PECVD) methods, reflecting a potential for industrial application; e.g. μc-SiC as the surface window layer for solar cells[56]. On the other hand, μc-SiC films prepared by SP methods have remained unexplored, until now. In a recent study, we reported the preparation of a μc-GeC:H film by introducing He during the sputtering process[61]. In this chapter, the author attempted to deposit μc-SiC:H films by MSP, and investigated the influence of He or H_2 addition during deposition on the optical, structural, and electrical properties of SiC:H films.

4.2 Experimental details

The first sputtering gas was methane (99.999% diluted to 50% by argon (99.9999%)), and the second sputtering gas, which was used to control the film properties, was either helium (99.9995%) or hydrogen (99.9999%). The partial pressure ratio (R) of helium gas to the total gas pressure was varied from 0 to 95%. The rf power, the sputtering pressure, and the substrate temperature were kept at 200 W, 3.7 Pa and 573 K, respectively, during the deposition of all films utilizing He. The deposition conditions under H_2 are described later. The substrates were glass plates (Corning 7059) for all measurements except the infrared spectrum (FTIR) measurements, for which silicon wafers were used.

The thickness of the deposited films was measured using a stylus instrument (TOKYO SEIMITSU: Surfcom 480). The X-ray diffraction measurements (Rigaku: RINT2000) used Cu Kα radiation. The optical absorption coefficient α from the visible to near-infrared range was obtained from the reflectance and transmittance data measured by a double-beam spectrophotometer (Jacso: V570) from 190 to 2500 nm. The IR transmittance spectra were measured by a Fourier transform infrared spectrophotometer (Jacso: FTIR 6100V) from 400 to 4000 cm^{-1}. The composition of the films was measured by an electron probe micro analyzer (EPMA; Shimadzu EPMA-1600) using an electron beam 0.1 mm in diameter, an acceleration voltage of 15 kV, and a sample current of 10 nA. The electrode used to measure the conductivity was formed in a

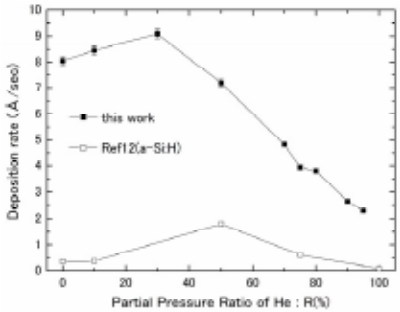

Fig. 4-1 Deposition rate (closed symbols) as a function of the partial pressure ratio *R* of helium to the total sputtering gas. The open symbols represent the data for a-Si:H from Ref. 62.

photocell-type configuration by evaporating aluminum onto SiC:H films. The temperature dependence of the DC conductivity was measured at temperatures of up to 523 K under a vacuum of 10^{-1} Pa.

4.3 Results and discussion

Figure 4-1 shows the deposition rate of Si_xC_{1-x}:H films as a function of the partial pressure ratio (*R*) of helium to the total gas pressure. With increasing *R*, the deposition rate increased, exhibiting a maximum at *R* = 30%. The appearance of a maximum in the deposition rate at *R* = 30% was also observed in our previous results involving a-GeC:H films[61]. These data have been interpreted as an increase in the argon ionization rate with helium dilution[62]. The deposition rate data from Ref. 62 are also plotted in Fig. 4-1. In Ref. 62, the authors reported an enhanced deposition rate of sputtered a-Si:H with a helium and argon gas mixture, where hydrogen with a partial pressure of only 4% was introduced as a reactive gas. The authors revealed that the total concentration of Ar ions in the plasma of He and Ar can be calculated by the product of the partial pressures of He and Ar, which reaches a maximum value when the two pressures are equal (*R* = 50%). In the present experiment, the partial pressure ratio of argon to helium is one-half of that in Ref. 62, since gas mixtures of argon (50%) and methane (50%) were used. Therefore, according to the procedure described in Ref. 62, we can deduce that the maximum value of the deposition rate in the present experiments appears at about *R* = 30%. The deposition rate decreases appreciably for *R* > 80%, which is caused by the increase of helium with low sputtering yield.

Figure 4-2 shows the film composition and the partial pressure ratio of methane as a function of *R*. The *R* dependence of the silicon content *x* tended to increase slightly with increasing *R* up to 70%, after which the carbon content 1–*x* decreased rapidly, with one exception at *R* = 80%. The decrease of 1–*x* for *R* > 70% could be due to the decrease in the partial pressure ratio of methane combined with the

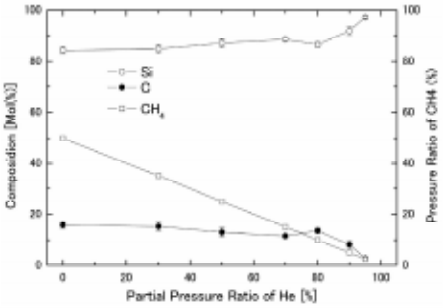

Fig. 4-2 Composition ratio of Si and C in deposited films, and the partial pressure ratio of methane under deposition.

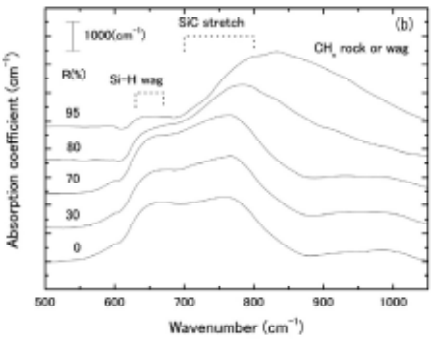

Fig. 4-3 Variation of IR absorption spectra in the range 500–1050 cm^{-1} with R.

increase in the ratio of helium. An explanation for the slight increase of $1-x$ at R = 80% is discussed later.

Figure 4-3 shows the variation of IR absorption spectra from 500 to 1050 cm^{-1} with R. For R = 0%, two strong bands were observed around 650 cm^{-1} and 750 cm^{-1}. The former band can be ascribed to the Si-H wagging vibration[63], and its intensity tended to decrease with increasing R, which is consistent with the results of Si-Hn stretching bands[50]. The latter band can be attributed to Si-C stretching modes[64], and its intensity tended to increase along with an increase in FWHM (full width at half maximum) with increasing R up to 80%, which implies an increase in the number of carbon atoms bonded to Si atoms. The observed peak shift of Si-Hn stretching bands[50] could be interpreted as an increase in the electro-negativity (Si: 1.4, C: 2.5[28]) of the nearest-neighbors of the Si atoms bonded to hydrogen atoms. Likewise, the increase in the composition ratio of carbon at R = 80% shown in Fig. 4-2 may reflect this increase in the number of carbon atoms bonded to Si atoms.

In addition to these tendencies, we can observe the broad band around 1000 cm^{-1} in detail; carbon related bands such as C-Hn wagging or rocking, 930 cm^{-1}; and/or C-C stretching, 1000 cm^{-1} [65,66]. The broad band becomes appreciable and merges into the Si-C stretching modes at R > 80%, which implies that the chemical decomposition of methane begins

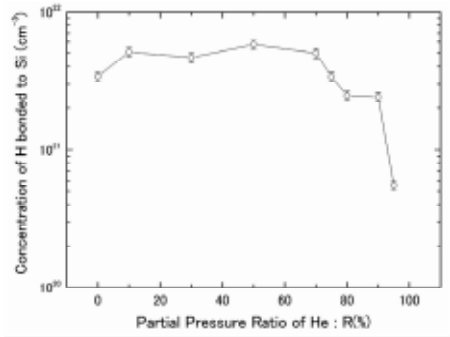

Fig. 4-4 Concentration of hydrogen bonded to Si (N_{Si-H}) as a function of R.

to overcome the physical sputtering of silicon, because of the low sputtering yield of He compared to Ar. This shift in the deposition process results in an increase in hydrocarbon species in the plasma, and therefore in the films, in which the bonding structure changes noticeably, as seen for R > 80%. This change in film structure is also reflected in the optical and electrical properties described later.

The concentration of hydrogen bonded to silicon (N_{Si-H}) is shown in Fig. 4-4. N_{Si-H} was approximately constant for R < 70%, for which the composition ratio of silicon shown in Fig.4-2 was also almost constant. The amounts of both silicon (deposition rate limited) and H (CH_4 dissociation rate limited) should decrease with increasing R, since the former is due to a decrease in the physical sputtering yield and the latter is due to a decrease in the partial pressure of methane. Despite these decreases in both elements, the constant N_{Si-H} suggests that the network structure of silicon not bonded to hydrogen becomes sparse. This interpretation may lead to an increase in the density of dangling bonds of silicon atoms, which will be discussed below for high R values.

N_{Si-H} decreased rapidly for R > 70%, which may have resulted from a reduction of the physical sputtering of silicon by argon in the plasma. Taking the compositional data shown in Fig.4-2 and the bonding behavior shown in Fig.4-3 for a high R into consideration, we could depict a structural model in which the amorphous network consists of Si atoms with a high density of dangling bonds along with a carbon related structure in which C atoms bond partially with these Si atoms. The concentration of hydrogen bonded to carbon was measured with great care using the C-Hn stretching band (2800–3000 cm^{-1}). Unfortunately, the spectra could not be distinguished clearly from the background signal, mainly because of the weak oscillator strength of the C-Hn stretching modes.

The optical band gap Eo is shown in Fig.4-5 together with the band-edge width factor B which is a constant representing the degree of disorder of the amorphous structure[7]. With increasing R, both Eo

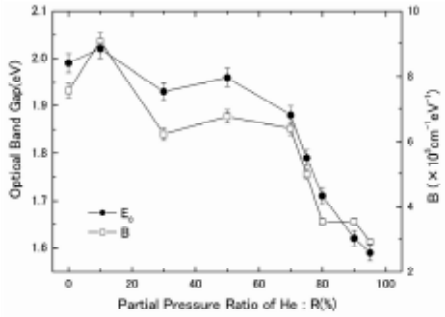

Fig. 4-5 Optical band gap Eo and the value B defined by $\alpha h\nu = B\,(h\nu - E\mathrm{o})^2$ (Tauc's formula[17]).

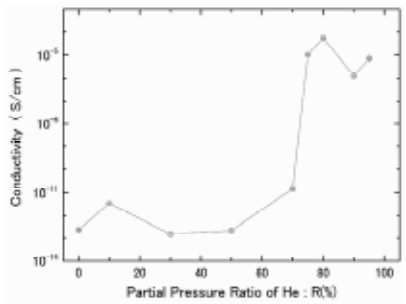

Fig. 4-6 D.c. conductivity σ_d at room temperature (294 K) as a function of R.

and B decreased gradually up to 70%, and then decreased rapidly for R > 70%. In amorphous semiconductors, a lower B value generally indicates a higher degree of structural disorder, which induces localized band tail states in the gap. Thus, B is inversely proportional to ΔE, where ΔE is the width of the band tail extending into the gap[17]. The rapid decrease in B implies that the Urbach tail-state's absorption increases, i.e., there was an appreciable increase in the density of band-tail states with increasing R. Generally, as for the hydrogenated binary amorphous semiconductors with a tetrahedrally bonded structure, Eo is affected by the concentration shift of each constituent elements. In Fig.4-2, the composition of films varies appreciably for R > 80%; the rapid decrease in carbon content is one cause of the decrease in Eo. Other important factors affecting Eo are the FWHM of the Si-C band in the IR spectra and $N_{\mathrm{Si-H}}$. Eo decreases generally with increasing FWHM and decreasing $N_{\mathrm{Si-H}}$ in amorphous SiC:H[67]. As shown in Fig.4-3, the FWHM increases with increasing R. Moreover, it is noteworthy that $N_{\mathrm{Si-H}}$ shows a significant reduction by about one order of magnitude for R > 80% in Fig.4-4. The decrease in $N_{\mathrm{Si-H}}$ causes network structural disorder and results in an increase in the Urbach band tail states. We therefore believe that the decrease in Eo was caused by these factors.

Figure 4-6 shows the dark d.c. conductivity σ_d at room temperature (294 K). σ_d increases by about six orders of magnitude for R > 70%. The abrupt

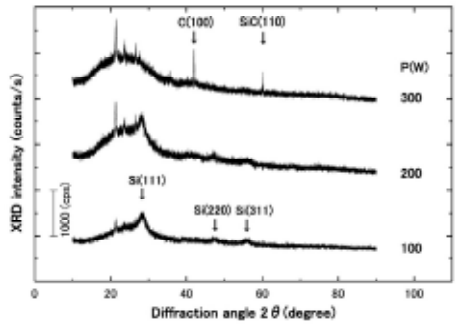

Fig. 4-7 Variation of X-ray diffraction pattern with rf power for films deposited with R = 90% of H_2.

increase of σ_d has also been observed for our a-GeC:H films[61], where it could be attributed to micro-crystallization, and in which the effectiveness of depositing crystallized films using light inert gases as sputtering ions has been investigated. We believe that for a-GeC:H, the rearrangement of ad-atoms at the substrate could be enhanced by decreasing the energy of the sputtering ion, which could facilitate micro-crystallization. In the present experiments, however, the deposited films had an amorphous nature, according to X-ray diffraction results for all samples. Moreover, as described above, the band-edge width factor B and $N_{\mathrm{Si-H}}$ both decreased considerably for R > 70%. Therefore, the abrupt increase of σ_d at RT can be ascribed to an increase in the density of band-tail states due to an increase in the degree of structural disorder accompanied by a decrease of bonded hydrogen.

In order to overcome this drawback for micro-crystallization using He, we tentatively attempted to utilize hydrogen instead of helium as a sputtering gas, taking our previous report on sputtered a-Si:H films into consideration[68]. In this case, the partial pressure ratio of the hydrogen gas to the total gas pressure was kept at R = 90%. The rf power was varied from 100 to 300 W, whereas the sputtering pressure and the substrate temperature were the same as in the experiments performed with He.

Figure 4-7 shows the rf power (P) dependence of the X-ray diffraction. The diffraction peaks were identified according to Powder Diffraction File-2 (PDF-2) (Release 2005/A of the International Center for Diffraction Data (ICDD)). The broadened diffraction peak around 2θ = 23° was mainly attributed to the amorphous nature of the films. The small peaks appearing in this diffraction angle range (21.5°, 23.7°, and 26.5°) originated from the argillaceous compound that affixes the specimen to be measured to the sample holder of the X-ray apparatus. It was found that the micro-crystalline structure formed within the amorphous structure. The peak of the diffraction line concerning Si is observable for P = 100 W and 200 W. For P = 300 W, although these peaks diminish, C(100) and

SiC(110) peaks appear. As measurements of the optical and electrical properties of these films are now in progress, a detailed report including a discussion of the validity of using hydrogen rather than helium as a sputtering gas will be published elsewhere.

CHAPTER 5 Superlatice formation[69)]

5.1 Introduction

Amorphous semiconductor superlattice (SL)s composed of alternating layers of wide-energy-gap materials (barrier layers) and narrow-gap materials (well layers) have been extensively investigated as new materials having interesting properties[70–72)]. In these studies, SLs have been generally prepared by the GD decomposition of source gases. In the GD method, a-SiC:H or a-SiN:H are generally used as barrier layers, and a-Si:H as a well layer. The latter is prepared from SiH_4 gas, and the former from the mixing of SiH_4 with hydrocarbon or NH_3 gas.

When a SL is prepared by using a one-chamber GD system, cross contamination from the residual gas is a serious problem[73)]; for example, in the preparation of the a-SiC:H/a-Si:H SL, the cross contamination of an a-Si:H layer arises from a minute amount of hydrocarbon gas existing in the reactor after an a-SiC:H layer deposition. This is a drawback of the GD method for synthesizing a SL, because it is important to form an abrupt compositional change at the interface between the wide-gap and the narrow-gap materials. In order to reduce this drawback, it is necessary to introduce a purge procedure of the reactor after a deposition of the barrier layer. As a result, the process of synthesizing the SL becomes complicated by many procedures[73)].

In the present chapter, we use a dual rf MSP system which had been designed for preparing multilayer films[74)]. In this method, the process for SL fabrication can be simplified, because the purge procedure of the reactor is not necessary, when two kinds of target materials are sputtered alternately in the same reactive gas. We have prepared a-SiC:H/a-GeC:H multilayer films using this SP method. The results concerning optical properties as well as periodic structural properties of a-SiC:H/a-GeC:H multilayer films are presented.

5.2 Sample preparation

Figure 5-1 shows a schematic diagram of the dual rf MSP system used for preparing amorphous multilayer films. A vacuum chamber is evacuated by an oil diffusion diffusion pump backed by a rotary pump. The chamber can be pumped down to 10^{-7} Torr. Two targets 80 mm in diameter are mounted at the lower part of the vacuum chamber.

Under each of these cathodes, a permanent ring-shape magnet is attached to a water-cooled magnet holder. The number of magnets in each magnet holder can be varied.

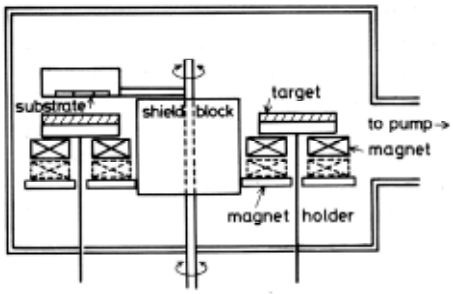

Fig. 5-1 Schematic diagram of a dual MSP system designed for preparing amorphous multilayer films.

Each target is alternately powered by an rf (13.56 MHz) power supply. Substrates are attached to a 8-cm-diam rotatable holder with a built-in heater, controlling the temperature of the substrates. The target-substrate distance can be set between 20 and 50 mm.

The substrate holder, which is connected to a shaft and a magnetic fluid feedthrough, is moved back and forth between two positions above these two targets and remains there during the deposition of a layer. A "shield block" is mounted between the two targets, which can prohibit the deposition of the sputtered particles on the other target. The pre-sputtering is performed for about 10 s, holding the substrate holder at the shield block. The deposition of one layer starts by a movement of the substrate holder from the shield block to the target. It ends with the moving of the substrate holder from the target to the shield plate, followed by turning the rf power off. The deposition of another layer starts with the moving of the substrate holder from the shield block to the position above the other target, after turning the rf power on and pre-sputtering.

In the present experiment, in order to deposit a-SiC:H/a-GeC:H multilayer films, a Si disk and a Ge disk are used for the deposition of an a-SiC:H layer and of an a-GeC:H layer, respectively. The size and the purity of the target are 80 mm in diameter and 5mm in thickness, and 99.999%, respectively, for both targets. The reaction gas is CH_4 diluted with Ar 50%–50%. The purities of constituent gas are 99.99% for CH_4 and 99.999% for Ar, respectively. The substrates are 9×18×0.5 mm fused quartz plates mounted on the substrate holder, which are held at 300 °C through the deposition of the multilayer film. The target-substrate spacing is 45 mm. After evacuation of the vacuum chamber below 5×10^{-6} Torr, the mixture gas of CH_4-Ar is introduced into the chamber.

The deposition rates of these films in the MSP method depend on several deposition conditions such as magnetic flux density, dilution rate of

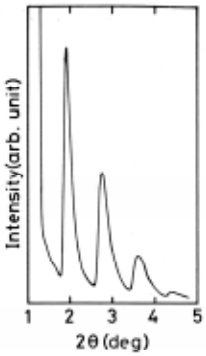

Fig. 5-2 Small-angle X-ray diffraction patterns vs scattering angle for a (aSiC:H 60 Å/a-GeC:H 20 Å)32 multilayer film.

reactive gas with inert gas, sputtering pressure, rf power, and substrate temperature[25,30]. In order to obtain a multilayer with well-defined sub-layers with an atomic scale, it is necessary to deposit each sub-layer at the low deposition rate. One of the conditions to satisfy this requirement is a reduction of magnetic flux density. In the present study, only one permanent magnet was attached to each magnet holder. The magnetic flux density in the immediate vicinity of each target is about 100 G.

The gas pressure is kept at 10 mTorr during sputtering, and the rf power to 200 W for the Si target and 50 W for the Ge target. For these conditions, the deposition rates are 2.4 and 2.6 Å s^{-1} for a-SiC:H and a-GeC:H, respectively. a-SiC:H layers of 60 Å thickness are deposited in 25 s, while the thickness of the a-SiGe:H layer is determined as follows. The composition of the films is periodically alternated between a-GeC:H (well layers) and a-SiC:H (barrier layers).

Several kinds of SLs were synthesized by changing the thickness of the well layer; the deposition time of an a-GeC:H layer was varied from 7 to 50 s, which corresponds to thicknesses from 20 to 130 Å. The total thickness of each multilayer film was kept at about 2600 Å. The corresponding number of layer pairs varies from 32 to 14. To characterize each layer, reference films of a-SiC:H and a-GeC:H of about 2600 Å thick were prepared. Optical and electrical properties of a-SiC:H and a-GeC:H films can be reffered in Ref.75.

5.3 Structural analysis

Small-angle X-ray diffraction (CuKa) was used to confirm the formation of the a-SiC:H/a-GeC:H multilayer. Fig. 5-2 shows an example of the X-ray diffraction peaks. More than three harmonic peaks can be observed for a (a-SiC:H 60 Å/a-GeC:H 20 Å)32 film, confirming the regular periodicity of the layered structure. The second Bragg reflection peak is observed at $2\theta = 1.91°$; the periodical length L of the multilayer structure is given by $\sin\theta = \lambda / L$, where θ is the refraction angle, λ the wavelength of the X-rays (1.5418 Å), and L the layer-repeat distance.

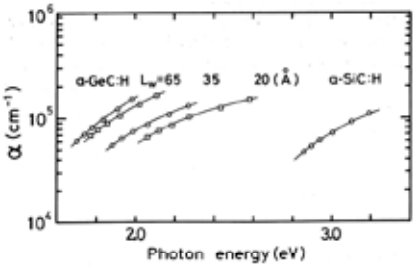

Fig. 5-3 Optical absorption coefficient vs photon energy for the SLs together with the reference films of a-SiC:H and a-GeC:H.

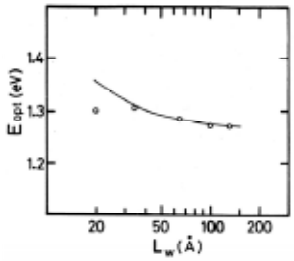

Fig. 5-4 Optical band gap of a-SiC:H/a-GeC:H SLs as a function of the thickness of the a-GeC:H layer (well layer).

We deduce a layer spacing L of 92 Å in agreement with the layer thickness determined from the deposition rates of the reference films. The thickness fluctuation of the interfaces between a-SiC:H and a-GeC:H was estimated from the FWHM of the peak. The measured FWHM of the second Bragg peak in the 28 scan for this 32-period structure is 0.16° (diffracto-meter resolution is 0.02°), corresponding to a thickness fluctuation of about 15Å for L = 92 Å. This value is larger than a reported value (7 Å for L = 80 Å) for an a-SiC:H/a-Si:H SL prepared by a GD method[76]. This is probably due to a high deposition rate (about 2.5 Å s^{-1}) in our MSP method, compared to the GD method (0.3–0.8 Å s^{-1}).

5.4 Optical bandgap

The optical absorption of a-SiC:H/a-GeC:H multilayer films was deduced from transmission measurements. The optical absorption coefficient α of multilayer films is shown in Fig.5-3 as a function of photon energy, together with the absorption data of reference films of a-SiC:H and of a-GeC:H prepared under the same conditions as the multilayer films.

The optical band gap E_{opt} was determined by fitting the absorption data using the Tauc's equation[17]. E_{opt} was plotted in Fig.5-4 as a function of the thickness of the a-GeC:H layer L_w. As L_w decreased below 100 Å, E_{opt} increased from the value of 1.26 eV for an a-GeC:H reference film. The

change of E_{opt} in this figure is explained by a simple quantum wen model: the separation of the lowest quantum effect level in the Kronig-Penny model, as given by

$$\Delta E_e = [h^2 /(8\pi^2 m_e^*)](\pi/L_w)^2,$$

where ΔE_e. m_e^*, and L_w are the energy-level shift from the conduction-band edge of the well layer, the effective electron mass, and the well layer thickness, respectively. m^*_e was assumed to be $0.8m_e$ (m_e is the electron mass). The energy level shift from the valence-band edge for holes is calculated in a similar way. In this case, the effective mass of holes is assumed to be equal to the electron mass[76]. The calculated result of E_{opt} including these energy-level shifts is also shown in Fig.5-4 (solid line), and is in good agreement with the experimental values.
This indicates that the synthesized films in this study exhibit the quantization effect. The deviation of the experimental value of E_{opt} for L_w = 20 Å from the calculated one is probably due to the thickness fluctuation described above.

6. CONCLUSIONS

(1) CHAPTER 1

1) Amorphous films of hydrogenated silicon-carbon alloys with excellent optoelectronic properties can be prepared by the MSP method using a silicon target and a gas mixture of argon and methane without using hydrogen.
2) The optical band gap and d.c. conductivity show marked changes with changing carbon content in the films upon varying the partial pressure of methane with respect to the total gas pressure.
3) The photoconductivity increases with increasing optical band gap up to 1.8 eV owing to the hydrogenation of silicon, and it decreases with further increase in the optical band gap owing to an increase in the density of localized states.
4) The photoconductivities in the films with optical band gaps above 1.9 eV are larger than those prepared by GD decomposition of silane and methane reported in the literature. This may be ascribed to the fact that the amount of hydrogen bonded to carbon in our films is small and that its bonding structure is relatively simple due to the deposition conditions of high power and low pressure, compared with the GD method.

(2) CHAPTER 2

1) With decreasing rf power, (i) activation energy of dark conductivity and of photoconductivity, and the optical band gap increase, (ii) the concentration of hydrogen bonded to carbon and the number of Si-C bonds increase, (iii) the parameter B and the refractive index decrease, and (iv) dark conductivity and photoconductivity decrease.
2) By examining the conduction band tail width and a factor of preferential attachment of hydrogen to carbon, these results are discussed from the standpoint of structural and compositional change of films with rf power originating mainly from the degree of decomposition of methane in the deposition process.
3) Comparing such characteristics as photoconductivity, the concentration of hydrogen bonded to carbon, and the preferential attachment factor, with those reported in the literatures for GD a-SiC:H, it is suggested that a relatively high degree of decomposition of methane is responsible for the excellent optoelectronic properties of the present films having the optical band gap above 1.9 eV.

(3) CHAPTER 3

1) Aluminum has been introduced into a-SiC:H by co-sputtering of silicon aluminum in a gas mixture of methane-argon In the range of fractional aluminum content z up to 10^{-2}, the photoconductivity was maintained without a significant change in the optical band gap.
2) A high value of photosensitivity (> 10^6) was obtained in the range of z between 10^{-4} and 10^{-3}. On increasing z above 10^{-2}, the photoconductivity is quenched, being accompanied by a decrease in the optical band gap as well as by an increase in the dark d.c. conductivity.

(4) CHAPTER 4

1) At high He partial pressure ratios R above 70%, the bonding configuration in the IR spectra changed; that is, the optical band gap decreased and the DC conductivity clearly increased. These data imply an increase in structural disorder caused by the introduction of a high R of He during sputtering.
2) In contrast to our previously reported GeC:H films, the micro crystallization of SiC:H films was found to be difficult when utilizing He. This drawback for micro crystallization could be improved by utilizing hydrogen instead of helium as a sputtering gas.

(5) CHAPTER 5

1) a-SiC:H/a-GeC:H SLs were fabricated using a dual MS method. The accuracy of the definition of multilayer films was confirmed by X-ray Bragg reflection. The quantization effect was observed in the well layer thickness dependence of the optical band gap.
2) The thickness fluctuation of the interfaces of the film was estimated to be 15 Å. This value is larger than a reported value for GD deposited SLs, which is probably ascribed to the large deposition rate of the present method.

References

(1) CHAPTER 1

1) N.Saito, T.Yamada, T.Yamaguchi, I.Nakaaki and N.Tanaka: Phil.Mag.B, Vol.52, pp.987-95, 1985.
2) Y.Tawada: Japan Annual Reviews in Electronics, Computers & Telecommunications, Vol.6, Amorphous Semiconductors Technologies Devices, edited by H.Hamakawa (Tokyo,Amsterdam: Ohmusha and North-Holland 1983) p.148; see also Y.Tawada, K.Tsuge, M.Kondo, H.Okamoto and Y.Hamakawa: J.Appl.Phys., Vol.53, pp.5273-81, 1982.
3) J.Bullot, M.Gauthier, M.Schmidt, M.Catherine and M.Zamouche: Phil.Mag.B, Vol.49, pp.489-501, 1984.
4) G.Moddel, J.Blake, R.W.Collins, P.Viktrovitch, D.K.Paul, B.Von Roedern and W.Paul: American Institute of Physics Conf.Proc, Vol.73, p.25, 1981.
5) T.D.Moustakas and R.Friedman: Appl.Phys.Lett., Vol.40, pp.515-7, 1982.
6) R.A.Roy and R.Messier: J.Vacuum Sci.Technoi., Vol.A2, p.312 1984.
7) R.Dutta, P.K.Banerjee and S.S.Mitra: Phys.Stat.Sol.(b), Vol.113, pp.227-84, 1982.
8) T.Shimada. Y.Katayama and K.F.Komatsubara: J.Appl.Phys., Vol.50, pp.5530-2, 1979.
9) A.Guvarc'h, J.Richard, M.Le Contellec, E.Ligeon and J.Fontenille: J.Appl.Phys., Vol.51, pp.2167-74, 1980.
10) H.R.Shanks, J.F.Ward and C.Carlone: J.Non-crystalline Solids, Vol.59-60, pp.581-4, 1983.
11) T.Thoda, K.Wasa and S.Hayakawa: J.Electrochem.Soc. Vol.127, pp.44-7, 1980.
12) N.Saito, H.Sannomiya, T.Yamaguchi and N.Tanaka: Appl.Phys.A, Vol.35, pp.241-7, 1984.
13) H.Shanks, C.J.Fang, L.Ley, M.Cardona, F.J.Demond and S.Kalbitzer: Phys.Stat.Sol.(b), Vol.100, pp.43-56, 1980.
14) F.Fujimoto, A.Ootsuka, K.Komaki, Y.Iwata, I.Yamane, H.Yamashita, Y.Hashimoto, Y.Tawada. K.Nishimura. H.Okamoto and Y.Hamakawa: Jpn.J.Appl.Phvs.,Vol.23, pp.810-4, 1984.
15) M.A.Bayne, Z.Kurokawa, N.U.Okorie, B.D.Roe and L.Johnson: Thin Solid Films, Vol.107, pp.201-6,1983.
16) H.Wieder, M.Cardona and C.R.Guarnieri: Phys.Stat.Sol. (b), Vol.92, pp.99-112, 1979.
17) N.F.Mott and E.A.Davis: Electronic Processes in Non-Crystalline Materials, second edition (Oxford: Clarendon Press,1979), p.289.
18) M.Cathkrine and G.Turban: Thin Solid Films, Vol.60, pp.193-200, 1979.
19) R.S.Sussman and R.Ogden: Phil.Mag.B, Vol.44, pp.137-58, 1981.
20) D.A.Anderson and W.E.Spear: Phil.Mag., Vol.35, pp.1-16,1977.
21) P.J.Zanzucchi, C.R.Wronski and D.E.Carlson, J.Appl.Phys., Vol.48, pp.5227-36, 1977.
22) N.Saito, Appl.Phys.Lett., Vol.46, pp.61-3, 1985.
23) A.Morimoto, T.Miura, M.Kumhda and T.Shimizu: J.Appl.Phys., Vol.53, pp.7299-305, 1982.
24) W.E.Spear, R.J.Loveland and A.Al-Sharbathy: J.Non-cryst.Solids, Vol.15, p.410, 1974.

(2) CHAPTER 2

25) N.Saito: J.Appl.Phys., Vol.58, pp.3504-7, 1985.
26) M.Le Contellec, R.Richard, A.Guivarc'h, E.Ligeon, and J.Fontenille, Thin Solid Films Vol.58, pp.407-11, 1979.
27) J.B.Webb, J.Appl.Phys. Vol.53, pp.9043-8, 1982.
28) G.Lucovsky: Solid State Commun., Vol.29, pp.571-6, 1979.
29) J.Saraie, Y.Fujii, M.Yoshimoto, K.Yamazoe, and H.Matsunami. Thin Solid Films Vol.117, pp.59-70, 1984.
30) See, for example, F.H.Field and J.L.Franklin, Electron Impact Phenomena (Academic, New York, 1970).
31) N.Saito: J.Appl.Phys., Vol.59, pp.2498-500, 1986.
32) N.Saito: J.Appl.Phys., Vol.61, pp.2962-5, 1987.
33) N.Saito: J.Non-Cryst.Solids, Vol.108, pp.211-5, 1989.
34) N.Saito: Philos.Mag.B, Vol.55, pp.615-25, 1987.

(3) CHAPTER 3

35) N.Saito, Y.Tomioka, T.Yamaguchi and K.Kawamura: Philos.Mag. Lett., Vol.59, pp.43-5, 1989.
36) M.G.Thompson and D.K.Reinhard: J.Non-cryst.Solids, Vol.37, pp.325-33, 1980.
37) T.Tanaka, K.Mori, S.Ishihara and S.Nagata: J.Vac.Soc.Japan, Vol.23, pp.571-6, 1980 (in Japanese).
38) ML Dayan, N.Croitoru and Y.Lereah: Phys.Lett.A, Vol.82, pp.306-8, 1981.
39) H.Niu, I.Yoshizawa, T.Shikama, T.Matsuda and M.Takai: Jap.J.Appl.Phys., Vol.23, pp.L18-20, 1984.
40) S.A.Abo-Namous, Y.Zaka and R.W.Fane: Thin Solid Films, Vol.125, pp.39-45, 1985.
41) H.S.Fortuna and J.M.Marshall: Phil.Mag.B, Vol.53, pp.383-90, 1986.
42) N.Saito: Appl.Phys.Lett, Vol.46, pp.61-3,1985
43) N.Saito, Y.Tomioka, H.Senda, T.Yamaguchi and K.Kawamura: Philos.Mag.B Vol.62, pp.527-36, 1990.
44) N.Saito, Y.Inui, T.Yamaguchi, I.Nakaaki: J.Appl.Phys., Vol.83, pp.2067-71, 1998.
45) N.Saito, Y.Inui, T.Yamaguchi and I.Nakaaki: Thin Solid Films, Vol.353, pp.189-93, 1999.
46) N.Saito, Y.Inui, T.Yamaguchi and I.Nakaaki: Thin Solid Films, Vol.281-2 pp.302-4, 1996.
47) Y.Tomioka, N.Saito, T.Yamaguchi and K.Kawamura: J.Vac.Soc.Jpn., Vol.33, pp.132-4; ibid pp.733-7, 1990 (in Japanese).
48) Y.Tomioka, N.Saito, T.Yamaguchi and K.Kawamura: J.Vac.Soc.Jpn., Vol.34, pp.351-3, 1991 (in Japanese).
49) N.Saito, T.Goto, Y.Tomioka, T.Yamaguchi and M.Shibayama: J.Appl.Phys. Vol.69, pp.1518-21, 1991.

(4) CHAPTER 4

50) N.Saito, M.Fujita, I.Nakaaki, S. Yamawaki, H.Iwata and K. Nishioka: J. Non-Cryst.Solids Vol.376, pp.81-5, 2013.
51) J.Meier, R.Flueckiger, H.Keppner and A.Shah: Appl.Phys.Lett., Vol.65, pp.860-2, 1994.
52) N.Saito, I.Nakaaki, H.Iwata and T.Yamaguchi: J.Vac.Soc.Jpn., Vol.46, pp.512-5, 2003 (in Japanese).
53) N.Saito, I.Nakaaki, S.Nakamura, S.Yoshioka and T.Yamaguchi: Appl.Surf.Sci., Vol.169-70, pp.472-5, 2001.
54) N.Saito, I.Nakaaki, H.Iwata and T.Yamaguchi: Thin Solid Films, Vol.515, pp.3766-71, 2007.
55) N.Saito, T.Yamaguchi and I.Nakaaki: J.Appl.Phys., Vol.78, pp.3949-54, 1995.
56) T.Chen, Y.Huang, A.Dasgupta, M.Luysberg, L.Houben, D.Yang, R.Carius and F.Finger: Solar Energy Materials and Solar Cells, Vol.98, pp.370-8, 2012.
57) J.Kouvetakis and J.W.Mayer: Silicon-Germanium Carbon Alloys, Growth, Properties and Applications (Taylor and Francis 2002), p.19; P.C.Kelires: ibid p.195;

B.-K.Yang, W.H.Weber and M.Krishnamurthy: ibid p.291.
58) D.L.Williamson: Solar Energy Materials and Solar Cells, 78, pp.41-84, 2003.
59) M.Boshta, B.Alavi, R.Braunstein, K.Barner and V.L.Dalal: Solar Energy Materials and Solar Cells, Vol.87, pp.387-393, 2005.
60) J.T.Herrold, and V.L.Dalal: J.Non-Cryst.Solids, Vol.270, pp.255-9, 2000.
61) N.Saito, H.Iwata, I.Nakaaki and K.Nishioka: Phys.Stat.Sol.A., Vol.206, pp.238-42. 2009.
62) M.S.Aida, N.Attaf, A.Benzegouta, L.Hadjeris, M.Selmi and O.Abdelwahab: Philso.Mag.Lett. Vol.76, pp.117-9, 1997.
63) P.J.Zanzucchi: Semiconductors and Semimetals Vol.21Hydrogenated Amorphous Silicon Part B (Academic Press 1984), p.121
64) H.Rubel, B.Schroder, B.Fuhs, J.Krauskopf, T.Rupp and K.Bethge: Phys.Stat.Sol.B., Vol.139, pp.131-43, 1987.
65) T.P.Drosedau, A.Annen, B.Schroder and H.Freistedt: Philso.Mag.B., Vol.69, pp.1-20, 1994.
66) M.Gazicki, H.Szymanowski, J.Tyczkowski, L.Malinovsky, J.Schalko and W.Fallmann: Thin Solid Films, Vol.256, pp.31-8, 1995.
67) D.K.Basa and F.W.Smith: Mat.Res.Soc.Symp.Proc., Vol.162, p.439, 1990.
68) N.Saito, H.Sannomiya, T.Yamaguchi and N.Tanaka: Appl.Phys.A., Vol.35, pp.241-7, 1984.

(5) CHAPTER 5

69) N.Saito and T.Yamaguchi: J.Appl.Phys., Vol.66, pp.3114-6, 1989.
70) B.Abeles and T.Tiedje: Phys.Rev. Lett., Vol.51, p.2003, 1983.
71) M.Hundhausen, P.Santos, L.Ley, F.Habraken, W.Beyer, R.Primig and G.Gorges: J.Appl.Phys., Vol.61, p.556, 1987.
72) T.Yoshimura, K.Hiranaka, T.Yamaguchi, and S.Yanagisawa: Philos.Mag. B Vol.55, p.409 1987.
73) S.Nishikawa, H.Kakinuma, T.Watanabe and K.Nihei: Jpn.J.Appl.Phys., Vol.25, p.1141, 1986.
74) T.Yamaguchi, H.Tamura, S.Taga and S.Tsuchiya: Appl.Opt., Vol.25, p.2703, 1986.
75) N.Saito, T.Yamaguchi and I.Nakaaki: J.Appl.Phys., Vol.78, pp.3949-54, 1995.
76) S.Tsuda, H.Tarui, T.Matsuyama, T. Takahama, S.Nakayama, T.Nishikawa, N.Nakamura, T.Fukatsu, M.Ohnishi, S.Nakano and Y.Kuwano: Jpn.J.Appl.Phys., Vol.26, p.28, 1987.

Received 19 February 2014;
received in revised form 8 April 2014;
accepted 9 April 2014.